Rapid-reaction kinetics of the bifurcating NAD$^+$-dependent NADPH:ferredoxin oxidoreductase NfnI from *Pyrococcus furiosus*

Received for publication, July 12, 2023, and in revised form, October 2, 2023 Published, Papers in Press, October 29, 2023,
https://doi.org/10.1016/j.jbc.2023.105403

Steve Ortiz[1], **Dimitri Niks**[1], **Seth Wiley**[2], **Carolyn E. Lubner**[2,*], **and Russ Hille**[1,*]

From the [1]*Department of Biochemistry and the Biophysics Graduate Program, University of California, Riverside, USA;* [2]*Biosciences Center, National Renewable Energy Laboratory, Golden, Colorado, USA*

Reviewed by members of the JBC Editorial Board. Edited by Joan B. Broderick

We have investigated the kinetics of NAD$^+$-dependent NADPH:ferredoxin oxidoreductase (NfnI), a bifurcating transhydrogenase that takes two electron pairs from NADPH to reduce two ferredoxins and one NAD$^+$ through successive bifurcation events. NADPH reduction takes place at the bifurcating FAD of NfnI's large subunit, with high-potential electrons transferred to the [2Fe-2S] cluster and S-FADH of the small subunit, ultimately on to NAD$^+$; low-potential electrons are transferred to two [4Fe-4S] clusters of the large subunit and on to ferredoxin. Reduction of NfnI by NADPH goes to completion only at higher pH, with a limiting k_{red} of 36 ± 1.6 s^{-1} and apparent K_d^{NADPH} of 5 ± 1.2 μM. Reduction of one of the [4Fe-4S] clusters of NfnI occurs within a second, indicating that in the absence of NAD$^+$, the system can bifurcate and generate low-potential electrons without NAD$^+$. When enzyme is reduced by NADPH in the absence of NAD$^+$ but the presence of ferredoxin, up to three equivalents of ferredoxin become reduced, although the reaction is considerably slower than seen during steady-state turnover. Bifurcation appears to be limited by transfer of the first, high-potential electron into the high-potential pathway. Ferredoxin reduction without NAD$^+$ demonstrates that electron bifurcation is an intrinsic property of the bifurcating FAD and is not dependent on the simultaneous presence of NAD$^+$ and ferredoxin. The tight coupling between NAD$^+$ and ferredoxin reduction observed under multiple-turnover conditions is instead simply due to the need to remove reducing equivalents from the high-potential electron pathway under multiple-turnover conditions.

Electron bifurcation involves the splitting of reducing equivalents from an obligate two-electron donor (typically a pyridine nucleotide), sending each of the individual electrons along separate high- and low-potential pathways, ultimately reducing high- and low-potential acceptors in a tightly coupled, thermodynamically favorable manner (1, 2). In this way, strongly reducing species such as reduced ferredoxin can be generated to act as the driving force for, for example, carbon and nitrogen fixation, among several other cellular processes in a variety of (mostly anaerobic) microorganisms. The final electron acceptor for the high-potential pathway must necessarily have a more positive reduction potential than the midpoint potential of the electron donor, and this difference provides the driving force for reduction of the low-potential acceptor. High-potential electron acceptors used by known electron bifurcating systems include crotonyl-CoA, caffeyl-CoA, pyruvate, NAD$^+$, and menaquinone; low-potential acceptors include ferredoxin and flavodoxin (1, 2).

The enzyme NAD$^+$-dependent NADPH:ferredoxin oxidoreductase (NfnI) is a structurally well-characterized example of an enzyme catalyzing electron bifurcation. The enzyme from *Thermotoga maritima* (3) or *Pyrococcus furiosus* (4) is a dimer comprised of large and small subunits, designated NfnL and NfnS, respectively (Fig. 1). NfnL contains the site of electron bifurcation, an FAD designated "L-FAD", along with two [4Fe-4S] clusters that together constitute the low-potential pathway; the cluster distal to the L-FAD is the site of ferredoxin reduction. NfnS contains a [2Fe-2S] cluster and a second FAD, the "S-FAD", that is the site of NAD$^+$ reduction, and together these two centers constitute the high-potential pathway (3, 4). The overall stoichiometry of the reversible transhydrogenation reaction catalyzed by the enzyme is:

$$2NADPH + NAD^+ + 2Fd_{OX} \leftrightharpoons 2NADP^+ + NADH + H^+ + 2Fd_{red}$$

A key feature of bifurcation in NfnI is that the half-potentials of the L-FAD are highly crossed (5), meaning the potential for the semiquinone:hydroquinone couple is much higher than that for the quinone:semiquinone couple, with the consequence that the semiquinone oxidation state is thermodynamically highly unstable (6). After the initial reduction of the L-FAD by NADPH (4), a high-potential electron is transferred to the high potential [2Fe-2S] cluster in the small subunit, leaving behind a very unstable and short-lived anionic semiquinone (FAD•$^-$) that has a sufficiently low reduction potential to pass its electron into the low potential pathway ultimately to ferredoxin (4). In the high-potential pathway, electron transfer from the now-reduced [2Fe-2S] cluster to the S-FAD yields a stable neutral semiquinone (FADH•), while a second equivalent of NADPH reacts at the bifurcating flavin,

* For correspondence: Russ Hille, rhille@ucr.edu; Carolyn E. Lubner, Cara.Lubner@nrel.gov.

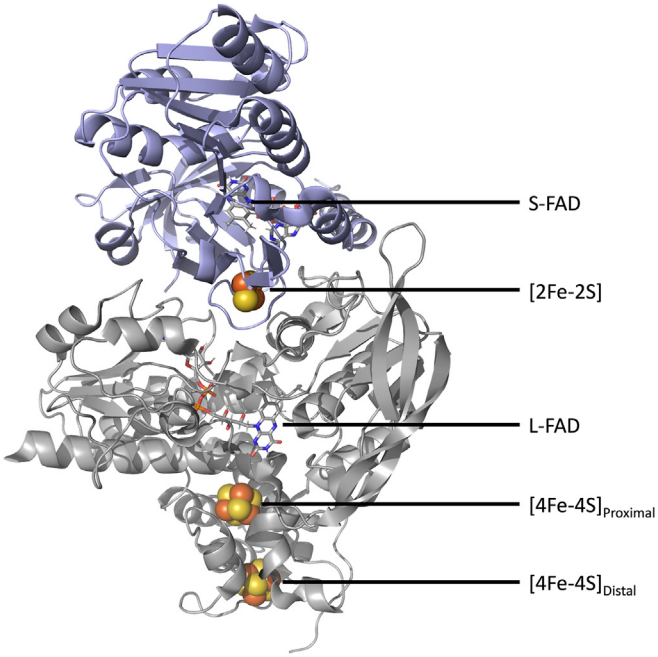

Figure 1. Structure of NfnI from *Pyrococcus furiosus* from the PDB 5JCA showing the cofactors in NfnL (*gray*) and NfnS (*blue*). NfnL (*gray*) contains the bifurcating L-FAD, and the low potential pathway consisting of the proximal and distal [4Fe-4S]. The L-FAD is able to preferentially bind NADPH through accommodation and stabilization of the phosphate group on NADPH. NfnS (*blue*) contains the high potential pathway of the [2Fe-2S] cluster and the terminal S-FAD that forms the stable FADH•. The S-FAD selectively binds NAD^+/NADH as a substrate due to the inability to accommodate the extra phosphate residue on NADPH causing steric hinderance in the active site.

introducing a second electron into each of the low- and high-potential pathways. The S-FAD becomes fully reduced to the hydroquinone anion ($FADH^-$) and is then able to reduce NAD^+ in a two-electron process. Thus, two bifurcation events are needed to reduce one equivalent of NAD^+ and two of ferredoxin. The bifurcation reaction is fully reversible, and the enzyme's transhydrogenase activity provides energy-conserving redox flow between the two pyridine nucleotide pools, thereby coordinating between catabolic and anabolic pathways of the cell.

The above notwithstanding, the exact basis for the tight coupling that is seen in reduction of the high- and low-potential acceptors during electron bifurcation remains unclear. In the present work, we have undertaken a rapid-reaction kinetic study of NfnI and characterized the reductive half-reactions with NADPH at the L-FAD and NADH at the S-FAD. The oxidative half-reaction has also been characterized, involving the reoxidation of pre-reduced NfnI with NAD^+. The reductive half-reaction work has been performed both in the absence and presence of ferredoxin, and we find that ferredoxin becomes reduced in the course of the reaction with NADPH even in the absence of NAD^+, albeit slowly (on a tens of second time scale). The yield of reduced ferredoxin is pH-dependent, increasing at higher pH (pH ∼ 9), where NADPH is a stronger reductant (7), and the yield of reduced ferredoxin approaches three per NfnI protomer. This implies that in the absence of NAD^+, NfnI is able to turn over as many as three equivalents of NADPH, filling the high-potential pathway with three high-potential reducing equivalents and providing three low-potential reducing equivalents for ferredoxin reduction. The three electrons that fill the high-potential pathway reside on the [2Fe-2S] cluster and the two e^- reduced $S\text{-}FADH^-$. This suggests that the bifurcating action of the L-FAD is intrinsically highly efficient and not strictly dependent on the simultaneous presence of the high- and low-potential acceptors. Instead, NAD^+ is required under steady-state conditions to remove reducing equivalents from the high-potential pathway. In addition, as previously identified crystallographically (3, 4) and by H/D exchange mass spectrometry (4, 8, 9), NAD^+ appears to induce a conformational change that significantly accelerates the rate of the initial electron transfer into the high potential pathway.

Results

pH dependence of the reductive half-reaction

Initial experiments examining the reductive half-reaction with NADPH at pH 7.5 were complicated by the fact that at lower [NADPH] (but still at stoichiometric excess), the enzyme was only incompletely reduced, becoming more so at higher [NADPH] due to mass action. The reduction potential of NADPH is quite pH-dependent, however, decreasing substantially as the pH is increased to ca. −400 mV at pH 9.5, 80 mV lower than −320 mV at pH 7.5 (7). NfnI is thus more readily reduced at higher pH. Indeed, at pH 9.5, the enzyme became fully reduced even at lower [NADPH] (Fig. S1). At pH 9.5, the observed rate constant exhibited a hyperbolic dependence on [NADPH], with a k_{red}^{app} of ∼36 ± 1.6 s^{-1} and an apparent K_d[1] of 5 ± 1.2 μM (Fig. 2*A*). The K_d for NADPH has been measured using fluorescence spectroscopy by Wise *et al.* (5), with a value of 3.0 ± 0.4 μM obtained at pH 8.8, in reasonable agreement with the present kinetic results at pH 9.5. NfnI was more extensively reduced at pH 9.5 than at pH 7.5 at any given [NADPH] although the extent of the absorbance change in the fast phase still increased at high [NADPH], indicating that the mass action effect remained (as expected, given the midpoint potential for the bifurcating L-FAD/$FADH^-$ of −436 mV at pH 8.8 (5)). At higher concentrations of NADPH, the transients exhibit biphasic behavior with the fast phase being responsible for approximately 30% of the total absorbance change (Fig. 3). The caveat regarding the extent of reaction being a function of [NADPH] notwithstanding, the rate constant for the fast phase of the reaction at pH 7.5 is still a hyperbolic dependence on [NADPH] (Fig. 2*B*) with a k_{red}^{app} of ∼113 ± 7.6 s^{-1} and apparent K_d of 8 ± 2.8 μM (these kinetic parameters must be considered apparent values only since at lower pH the reaction does not go to completion). Still, the only modest pH-

[1] As rigorously demonstrated by Strickland *et al.* (17)—the rapid-reaction kinetic approach used here yields a proper dissociation constant, as defined by k_{-1}/k_1 for the reversible binding of the substrate. In the present case, however, more than one process appears to be taking place subsequent to the initial substrate binding event, and for this reason, we refer to the parameter here as an *apparent* K_d.

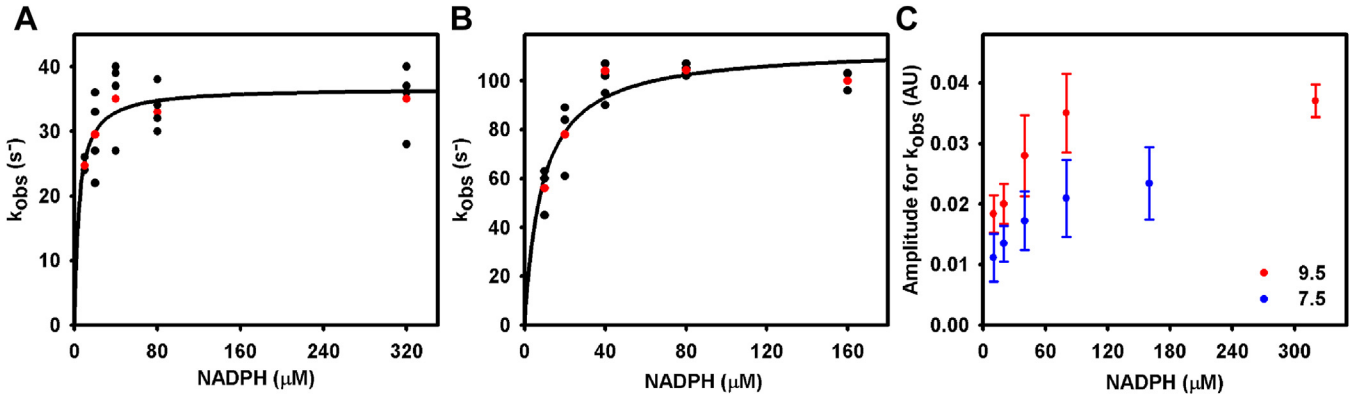

Figure 2. Reductive half-reaction kinetics of NfnI with NADPH at pH 9.5 and 7.5. The data points at each [NADPH] reflect the rate of the fast phase of the reductive half-reaction in (*A* and *B*). *A*, plot of k_{obs} *versus* [NADPH] at pH 9.5 with the *red* points indicating the average of the separate trials. The hyperbolic fit yielded a k_{red} of 36 ± 1.6 s^{-1} and apparent K_d of 5 ± 1.2 μM. *B*, plot of k_{obs} *versus* [NADPH] at pH 7.5 with the *red* points indicating the average of the separate trials. The hyperbolic fit yielded a k_{red} of 113 ± 7.6 s^{-1} and apparent K_d of 8 ± 2.8 μM. Both experiments involved mixing 5 μM NfnI with varying concentrations of NADPH over the range 10 to 320 μM. *C*, averages of the total change in amplitude attributed to the fast phase of the reaction of enzyme with NADPH, at 450 nm, from panels A and B at pH 9.5 (*red*) and pH 7.5 (*blue*), respectively. This indicates that ∼3.5 μM L-FAD is reduced at pH 9.5, whereas at pH 7.5, it is closer to ∼2.5 μM L-FAD, with a $\Delta\varepsilon_{450\ nm}$=10 mM^{-}cm^{-} for the L-FAD.

dependence of k_{red} (see also Fig. S1) indicates that there is no significant acid-base catalysis involved in the initial hydride transfer to the L-FAD from the NADPH. Also shown in Figure 2*C* are averages of the total absorbance change attributed to the fast phase of L-FAD reduction by NADPH, collected at pH 9.5 (red) and 7.5 (blue), illustrating the more extensive reduction of NfnI at pH 9.5 than pH 7.5. At pH 7.5, the amplitude of the fast phase of the reaction continues to increase over the range 40 to 160 μM NADPH when the rate constant itself has saturated (Fig. 2*B*), whereas at pH 9.5, the change in amplitude is better-behaved and saturates at approximately the same [NADPH] as seen for the observed rate of reduction (Fig. 2, *A* and *C*). This behavior is indicative of the more favorable thermodynamic drive of NADPH to reduce the L-FAD at higher pH values where its reduction potential is lower.

The extent of reduction in the fast phase of the reaction of NfnI with NADPH increases without a dramatic decrease in the apparent k_{red} of the reaction at pH 9.5, when compared to the same saturating concentration at pH 7.5. This phase of the reaction reflects reduction of the L-FAD by NADPH as evidenced by the difference spectrum shown in Figure 3*B* (blue spectrum) and accounts for approximately 30% of the total absorbance change seen at 450 nm (Fig. 3). This 30% of total absorbance change accounts for 60% of the total amount of L-FAD becoming reduced within the fast phase of the reaction. NADPH is able to exclusively bind to and reduce the central L-FAD due to the presence of amino acid residues in the active site that are able to stabilize the negative phosphate group present in the substrate as shown in the X-ray crystal structure, which are absent in the S-FAD active site (3). Some electron transfer out of the now-reduced L-FADH^{-} may also have begun in the course of the fast phase of the reaction, leading ultimately to reduction of the S-FAD to FADH• in the high-potential pathway, as reflected in the small absorbance increase in the 540 to 660 nm region over the first 150 ms of the reaction (Fig. 3*B*, Inset). We attribute the transient long-wavelength absorbance increase to accumulation of the S-

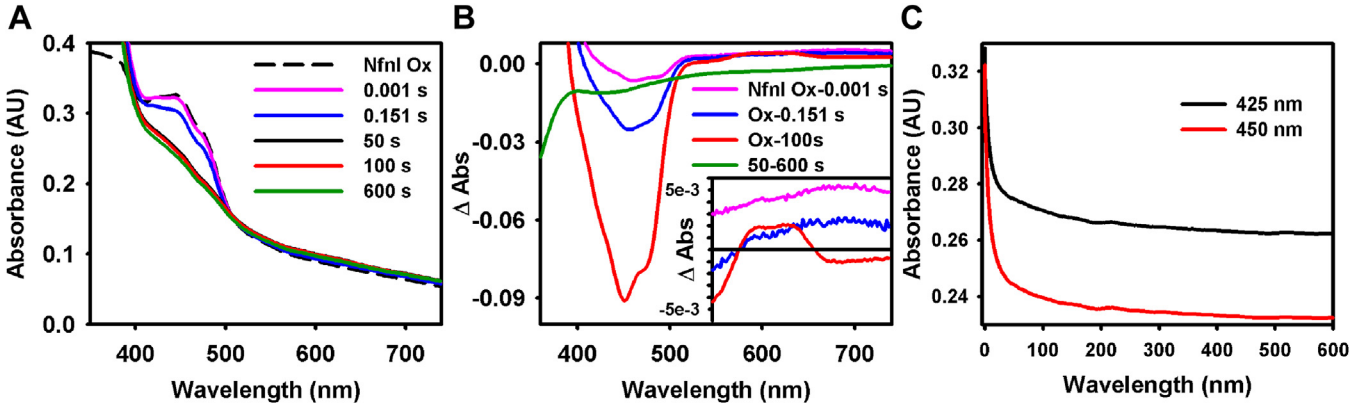

Figure 3. The spectral changes associated with the reduction of 6 μM NfnI with 200 μM NADPH at pH 9.5. *A*, shown are spectra at the end of the mixing deadtime (*magenta*), the end of the fast phase (*blue*), the 50 s time point (*solid black*), the 100 s time point (*red*), and completion of reaction (*green*). *B*, difference spectra generated by subtracting the spectra at time points shown in the figure legend. *Inset:* difference spectra enlarged in the 540 to 740 nm region to show the absorption that is attributed to accumulation of the S-FADH•. *C*, shown are the 425 nm (*black*) and the 450 nm (*red*) transients of the course of the reaction.

FADH• as the S-FAD is known to form the blue, neutral semiquinone, and the reaction of NADPH with the L-FAD is known not to generate a long-wavelength–absorbing charge-transfer complex (4). This electron transfer, however, is a fraction of the overall absorbance change during the 151 ms and develops more prominently over the time course of the 100 s. The point is that there is a single reduction event whose extent is in equilibrium (between NADPH and L-FAD on the one hand and $NADP^+$ and L-$FADH^-$ on the other) and thus dependent on [NADPH] due to mass action.

Subsequent to the fast phase of the reaction, S-FADH• accumulates maximally at ∼5 s after mixing and then decays, the S-FAD becoming fully reduced to the S-$FADH^-$ as more equivalents of NADPH react with the enzyme over the next few hundred seconds; the low-potential [4Fe-4S] clusters become reduced on approximately the same time scale. After the first electron oxidation of the fully reduced L-$FADH^-$, a red $FAD•^-$ is formed; the semiquinone left behind decays within a matter of picoseconds, due to the low reduction potential of −911 mV, and is only observed using picosecond transient absorbance spectroscopy (4). The change in absorbance attributed to iron-sulfur reduction is not very great at 425 nm (green spectrum in Fig. 3*B*) and does not develop independently of the larger changes associated with flavin reduction until after 50 s, possibly due to intermolecular electron transfer on such long-time scales (see Discussion). Although the reduction of the [4Fe-4S] cluster produces a maximum change at 425 nm, the behavior of the 425 nm transient follows that of the monitored 450 nm used to follow the initial FAD reduction (Fig. 3*C*). The observed very long-time scale on which these slowest processes occur in turn implies that in the absence of any terminal electron acceptors, the low-potential electrons generated in the bifurcating event migrate only very slowly into the high-potential pathway. Although this entails reoxidation of the low-potential iron-sulfur clusters, under the reaction conditions with excess NADPH, they immediately become re-reduced in the reaction with additional NADPH.

Ferredoxin reduction in the course of the reductive half-reaction of NfnI

We next examined the kinetics of ferredoxin reduction by NfnI in both the absence and presence of the high-potential acceptor NAD^+. The UV/visible absorption change associated with ferredoxin reduction is difficult to resolve in the 400 nm region, although a careful analysis of the difference spectra before and after reduction permitted quantitation of the amount of ferredoxin reduced (Figs. 4 and 5). A UV/visible difference spectrum indicative of ferredoxin reduction has a maximum at 420 nm, and if enough ferredoxin was reduced, the longer wavelength band in the 600 to 750 nm region can also be seen (Fig. S2*A*). Using this criterion and a $\Delta\varepsilon_{420\ nm}$ = 8.3 $mM^{-1}\ cm^{-1}$ (Fig. S2*A*), the amount of ferredoxin reduced from a difference spectrum could be estimated. Given the uncertainties in the analysis of the UV/visible absorption changes, ferredoxin reduction was also quantified by electron paramagnetic resonance (EPR) (Fig. 6, *A* and *B*) using dithionite-reduced *Megasphaera elsdenii* ferredoxin as an integration standard (Fig. 6*C*). We chose the ferredoxin from *M. elsdenii* rather than *P. furiosus* due to its better-resolved EPR signal as compared to the *P. furiosus* ferredoxin (10). In particular, the well-resolved g_1 feature (g_1 = 2.074) of the *M. elsdenii* ferredoxin does not overlap with any EPR features of the iron-sulfur clusters of the *P. furiosus* NfnI, significantly simplifying quantification of reduced ferredoxin. To ensure that using *M. elsdenii* ferredoxin did not alter the kinetics and inherent properties of the NfnI reaction, the rapid-reaction kinetic and EPR experiments described below were repeated in tandem with ferredoxins from both organisms as were steady-state assays, all of which indicated that the two are equally effective as low-potential acceptors for NfnI. A comparison of the rapid-reaction kinetic behavior is shown in Fig. S3.

In the presence of ferredoxin but absence of the high-potential acceptor, NAD^+, NfnI can in principle undergo three successive bifurcation events. The three equivalents of NADPH that can successively reduce NfnI; in total, send three electrons into the high-potential pathway to fully reduce the [2Fe-2S] cluster and the S-FAD and three electrons to the low-potential pathway which can be passed on to three ferredoxins. Indeed, significant ferredoxin reduction by NfnI occurs with NADPH (and in the absence of NAD^+), but the yield is pH-dependent. At pH 7.5, NADPH-reduced NfnI is able to reduce a single equivalent of ferredoxin in 600 s (Figs. 4*A*, inset and 6*A*). After NfnI is initially reduced by NADPH in the fast phase, the ferredoxin slowly becomes reduced as shown in the shallow change in the 450 nm trace (black) in Figure 4*C*. Once 200 μM NAD^+ is introduced, the reaction proceeds at a much faster rate with the most reduced point in the 450 nm transient shown in Figure 4*C* appearing at ∼17 s. The stoichiometry of the reaction also increases to approximately four equivalents of ferredoxin reduced per NfnI (Fig. 6*B*). These stoichiometries probably underestimate the true yield, as after 17 s, the ferredoxin begins to reoxidize, most likely due to back electron transfer to NfnI (Fig. 4*C*). This reoxidation is apparent in the transients seen at 450 nm where ferredoxin reoxidation is manifested as an absorbance increase with a maximum at 420 nm (Fig. 4*B*, blue spectrum in inset). At pH 9.5, the stoichiometry for ferredoxin reduction in the absence of NAD^+, as measured by EPR, increases to 2.3 equivalents per NfnI (Fig. 6*A*), in rough agreement with the value of 3 obtained by UV/visible spectroscopy, and in the presence of NAD^+, the equilibrium shifts toward reducing the remaining ferredoxin (Fig. 6*B*), with no electron transfer back to NfnI (Fig. 5*C*, red transient). The difference in the level of ferredoxin reduction in the absence of NAD^+ is made clear in Figure 6*A*, which shows that the EPR signal intensity of reduced ferredoxin is greater at pH 9.5 than pH 7.5. The back electron transfer from ferredoxin (presumably to the low potential [4Fe-4S] clusters of NfnI) seen at pH 7.5 reflects the ability of NfnI to catalyze confurcation and may explain why no more than four equivalents of ferredoxin are transiently reduced in the bifurcating direction with saturating amounts of all three substrates (Fig. 4*C*, red spectrum). It is important to point out that the

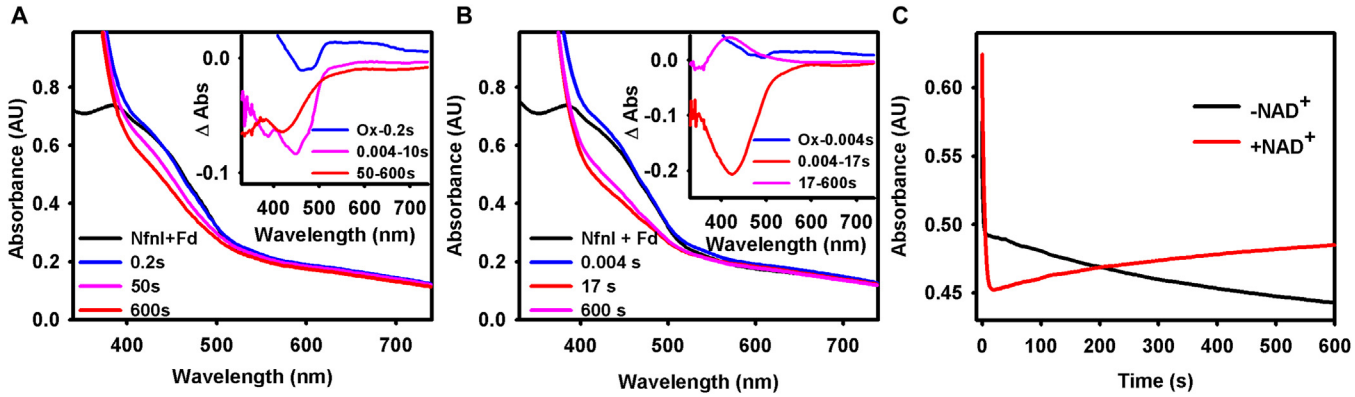

Figure 4. Rapid reaction kinetics of the reduction of *Megasphaera elsdenii* ferredoxin at pH 7.5. The spectra shown reflect the starting point of the reaction in the form of the oxidized spectrum, the initial time point after mixing or the end of the fast phase of the reaction, and lastly, the most reduced point of the 450 nm trace. *A*, spectra for ferredoxin reduction in the absence of NAD^+ with the oxidized spectrum (*black*), the 0.2 s time point (*blue*), the 50 s time point (*magenta*), and most reduced spectrum at 600 (*red*). *Inset*: difference spectra generated by subtracting the spectra at time points shown in the figure legend. *B*, spectra for ferredoxin reduction in the presence of NAD^+ with the oxidized spectrum (*black*), the first time point (*blue*), the most reduced spectrum (*red*), and the 600 s time point (*magenta*). *Inset*: difference spectra generated by subtracting the spectra at time points shown in the figure legend. *C*, traces extracted at 450 nm from the ferredoxin reduction experiments in panels *A* and *B*; this wavelength was chosen to monitor both ferredoxin and NfnI reduction. The 450 nm trace in the absence of NAD^+ (*black*) has a longer mixing dead time effect and as a result begins at lower starting point than the other trace shown. All experiments were performed with 5 μM NfnI and 25 μM ferredoxin in the presence of 200 μM NADPH and ± 200 μM NAD^+ at 30 °C. All experiments were monitored over a 600 s time period.

reaction at pH 9.5 takes more than 100 s to go to completion, a point considered further in the Discussion. The higher yield of reduced ferredoxin at higher pH in the absence of NAD^+ is again most likely due to the increased thermodynamic driving force for reduction at the higher pH.

We next examined the reaction of ferredoxin with dithionite-reduced NfnI. At pH 9.5, the sample was frozen within a second of mixing for EPR quantification of ferredoxin reduction. As shown in Figure 7, approximately one equivalent of ferredoxin was reduced. The spectrum also includes signals from the FADH• and the [2Fe-2S] cluster of the high-potential pathway (4). In the absence of excess dithionite, only one of the two [4Fe-4S] clusters of the low-potential pathway becomes reduced, presumably the distal cluster with the reduction potential of −513 mV since only one equivalent of ferredoxin is reduced in the reaction (4). Thus, reduction of ferredoxin appears not to be rate-limited by electron transfer from the low potential [4Fe-4S] distal cluster to the ferredoxin. This implies that even a partially reduced low-potential pathway will rapidly reduce ferredoxin without the need for generating the extremely low potential electron (−911 mV (4)) from the bifurcating L-FAD.

The reductive half-reaction with NADH in the absence and presence of ferredoxin at pH 9.5

NADH readily binds to and reduces the S-FAD of the high-potential pathway in the reverse of the bifurcation reaction. Unlike the reaction with NADPH, the reaction with NADH is more well-behaved with well-resolved kinetic phases. The rate constant for the fast phase of the reaction exhibits a

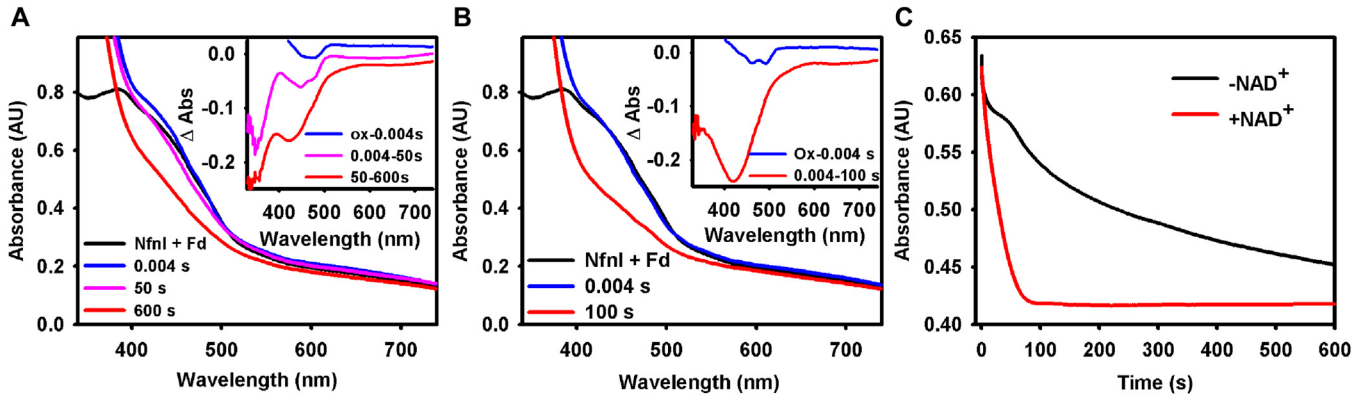

Figure 5. Rapid reaction kinetics of the reduction of *Megasphaera elsdenii* ferredoxin at pH 9.5. The spectra shown reflect the starting point of the reaction in the form of the oxidized spectrum, the initial time point after mixing or the end of the fast phase of the reaction, and lastly, the most reduced point of the 450 nm trace. *A*, spectra for ferredoxin reduction in the absence of NAD^+ with the oxidized spectrum (*black*), the first time point 0.004 s (*blue*), the 50 s time point (*magenta*), and the most reduced spectrum at 600 s (*red*). *Inset:* difference spectra generated by subtracting the spectra at time points shown in the figure legend. *B*, spectra for ferredoxin reduction in the presence of NAD^+ with the oxidized spectrum (*black*), the first time point (*blue*), and the most reduced spectrum (*red*). *Inset:* difference spectra generated by subtracting the spectra at time points shown in the figure legend. *C*, traces extracted at 450 nm from the ferredoxin reduction experiments in panels *A* and *B*; this wavelength was chosen to monitor both ferredoxin and NfnI reduction. All experiments were performed with 5 μM NfnI and 25 μM ferredoxin in the presence of 200 μM NADPH and ± 200 μM NAD^+ at 30 °C. All experiments were monitored over a 600 s time period.

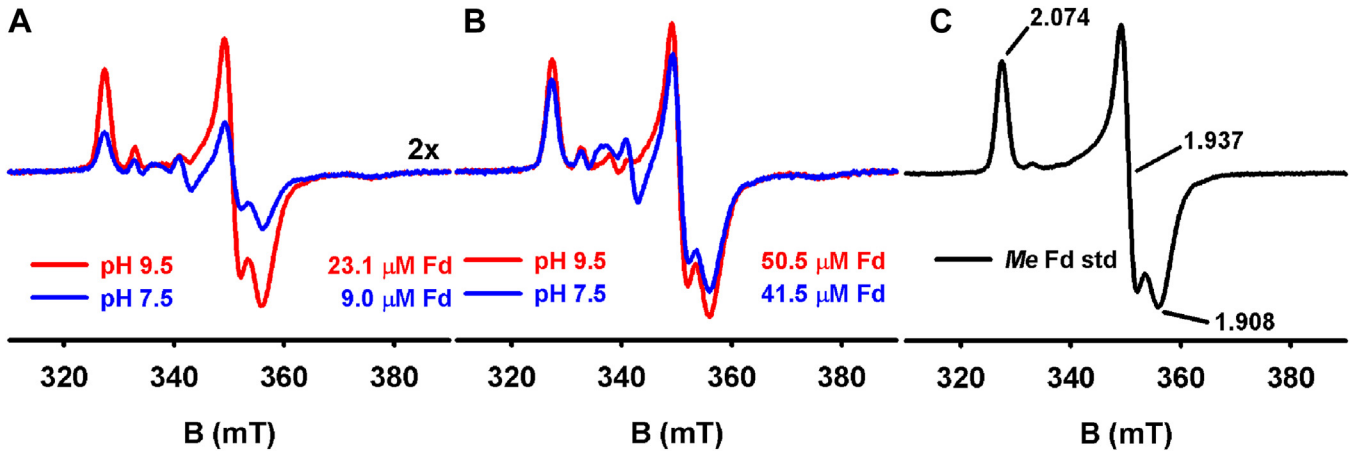

Figure 6. Quantification of ferredoxin reduction by EPR. All experiments were performed with 10 μM NfnI and 50 μM ferredoxin in the presence of 400 μM NADPH and ± 400 μM NAD^+ with incubation at 30 °C over the course of the reaction. *A*, EPR spectra for the reduction of *Megasphaera elsdenii* ferredoxin in the absence of NAD^+. Samples were frozen at 600 s at both pH 7.5 (*blue* spectrum) and pH 9.5 (*red* spectrum). The incubation time reflects maximum accumulation of reduced ferredoxin as determined in Figures 3*A* and 4*A*, respectively. Spectra were enlarged 2× for clarity. *B*, EPR spectra for the reduction of *M. elsdenii* ferredoxin in the presence of 400 μM NAD^+. Samples were frozen at 17 s at pH 7.5 (*blue* spectrum) or 100 s at pH 9.5 (*red* spectrum). The incubation time reflects maximum accumulation of reduced ferredoxin as determined in Figures 3*B* and 4*B*, respectively. The spectra were scaled to reflect 40% nonfunctional protein. *C*, spectrum of 50 μM *M. elsdenii* ferredoxin integration standard ($g_{1,2,3}$ = 2.074, 1.937, 1.908) was used to quantify the amount of reduced ferredoxin present in each of the samples above. All of the data was collected at 15 K with 1 mW power and 1 mT modulation amplitude. EPR, electron paramagnetic resonance.

hyperbolic dependence on [NADH], yielding a k_{red}^{app} of 205 ± 1.9 s^{-1} and an apparent K_d of 29 ± 1.1 μM for NADH; the wavelength dependence of this phase clearly indicates that it is due to flavin reduction (Fig. 8*B*, *inset*). The better-behaved reductive half-reaction of the S-FAD may be due in part to the fact that the reduction occurs in a single phase with electron transfer from the fully reduced S-$FADH^-$ to the [2Fe-2S] cluster being much slower and thus better resolved from the initial reduction of the S-FAD. The fast phase is followed by an intermediate phase with an [NADH]-independent rate constant of 0.24 s^{-1} whose wavelength dependence exhibits an equilibrium between S-$FADH^-$/$[2Fe\text{-}2S]_{ox}$ and S-FADH•/$[2Fe\text{-}2S]_{red}$ within the high-potential pathway. Finally, in a slow phase, the long wavelength absorbance of the FADH• is lost as the S-FAD becomes fully reduced (Fig. 8*B*). The addition of oxidized ferredoxin to the reaction mix does not increase the rate of reduction of the S-FAD, but at longer timescales, the reducing equivalents introduced by NADH are able to reduce ferredoxin at a slower rate than seen with NADPH (Fig. S4). This implies that pairs of reducing equivalents in the high-potential pathway can make their way back to the bifurcating L-FAD which might then bifurcate normally and send one electron on to the low-potential pathway to reduce ferredoxin. Alternatively, the reduction of ferredoxin by NADH may be due to the NADH binding to the L-FAD, directly enabling a bifurcation event. The possibility of NADH binding at the L-FAD is supported by the crystal structure of *T. maritima* NfnI in which NAD^+ is found adjacent to the L-FAD active site upon soaking crystals with excess NAD^+ (3). In one of the two protomers of the asymmetric unit, NAD^+ is bound adjacent to the S-FAD of the high-potential pathway, as expected, but in the other protomer, NAD^+ is bound at the bifurcating L-FAD, suggesting that direct reduction of the bifurcating center by NADH may be possible. In addition, H/D exchange mass spectrometry has shown that NADH binding alters backbone exchange in the vicinity of the L-FAD (4, 8, 9).

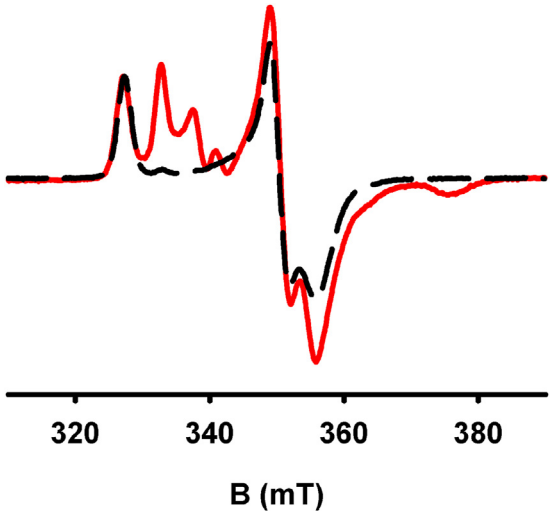

Figure 7. Quantification of ferredoxin reduction by EPR with pre-reduced $NfnI_{red}$. Twenty micromolars of NfnI was pre-reduced with sodium dithionite (no excess) prior to reaction with 100 μM *Megasphaera elsdenii* ferredoxin. The sample was frozen within a second of mixing (*red* spectrum). Spectrum of *M. elsdenii* ferredoxin integration standard ($g_{1,2,3}$ = 2.074, 1.937, 1.908) used to quantify the amount of reduced ferredoxin present in the reaction which was determined to be 18.8 μM. The integration standard spectrum was scaled for reference (dashed black spectrum). The residual spin density from NfnI present in the sample spectrum reflects contributions predominantly from the FADH• (g = 1.999) and the [2Fe-2S] ($g_{1,2,3}$ = 2.047, 1.915, 1.805); of note is the apparent electron–electron interaction between the FADH• and the adjacent [2Fe-2S] (4). The spectra were collected at 15 K with 1 mW power and 1 mT modulation amplitude. EPR, electron paramagnetic resonance.

The oxidative half-reaction of $NfnI_{red}$ with NAD^+ at pH 9.5

We next examined the reaction of pre-reduced NfnI with NAD^+. The fast phase of the reaction exhibits a rate constant

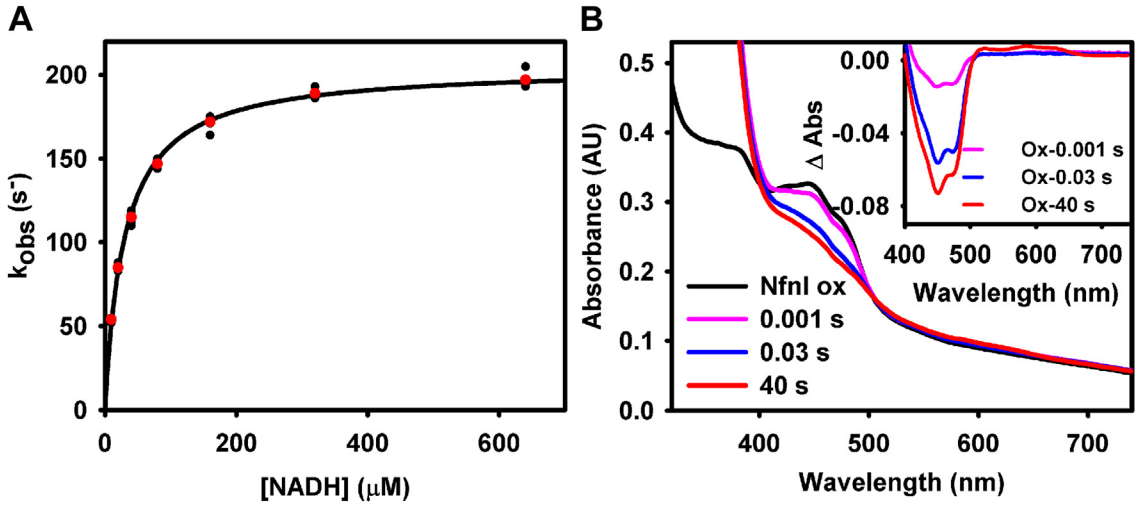

Figure 8. Reductive half-reaction kinetics of NfnI with NADH at pH 9.5. *A*, plot of k_{obs} *versus* [NADH] with the *red* points depicting the average of the separate trials. The hyperbolic fit yielded a k_{red} of 205 ± 1.9 s^{-1} and apparent K_d of 29 ± 1.1 μM. The experiment involved mixing 6 μM NfnI with varying concentrations of NADH over the range 10 to 640 μM. *B*, the reduction of 6 μM NfnI with 200 μM NADH. The oxidized NfnI (*black* spectrum), first time point (*magenta* spectrum), the end of the fast phase (*blue* spectrum), and the time at which maximum FADH• accumulates (*red* spectrum) are shown. *Inset:* difference spectra generated by subtracting the spectra at time points shown in the figure legend.

that has a hyperbolic dependence on [NAD^+], yielding a k_{ox} of 50 ± 0.7 s^{-1} and apparent K_d of 8 ± 0.6 μM at pH 9.5, with the spectral change indicating that only the S-FAD becomes oxidized in an obligatory two-electron process. The spectral features can be attributed solely to the reoxidation of the S-FAD, due to the single phasic nature of the 450 nm transient (Fig. 9*B*, inset) and the clearly resolved 450 nm band in the difference spectrum in Figure 9*C*. Only more slowly does FADH• begin to accumulate, indicating at least partial electron transfer from the [2Fe-2S] cluster to the now reoxidized S-FAD, as reflected in the absorbance increase in the 550 to 660 nm region, Figure 9*C*. In addition, the inset of Figure 9*C* illustrates that the 580 nm transient used to monitor FADH• formation is not a well-behaved exponential over the 100 s of the reaction, and a reliable k_{obs} cannot be extracted. In a parallel EPR experiment, accumulation of FADH• can be seen during steady-state turnover (Fig. 6*B*), indicating again that after oxidation of the S-FAD, there is some electron transfer from the [2Fe-2S] cluster to the flavin in the high-potential pathway. The amount of FADH• observed is pH-dependent, as expected, with more FADH• accumulating at pH 7.5 than at pH 9.5. The reaction is not expected to proceed further than the two-electron oxidation of the high-potential pathway, as further NAD^+ reduction would require either electron bifurcation at the reduced L-$FADH^-$ (impossible with the low-potential pathway filled) or electron transfer from the low- to the high-potential pathway (representing a short-circuit reaction which would defeat bifurcation).

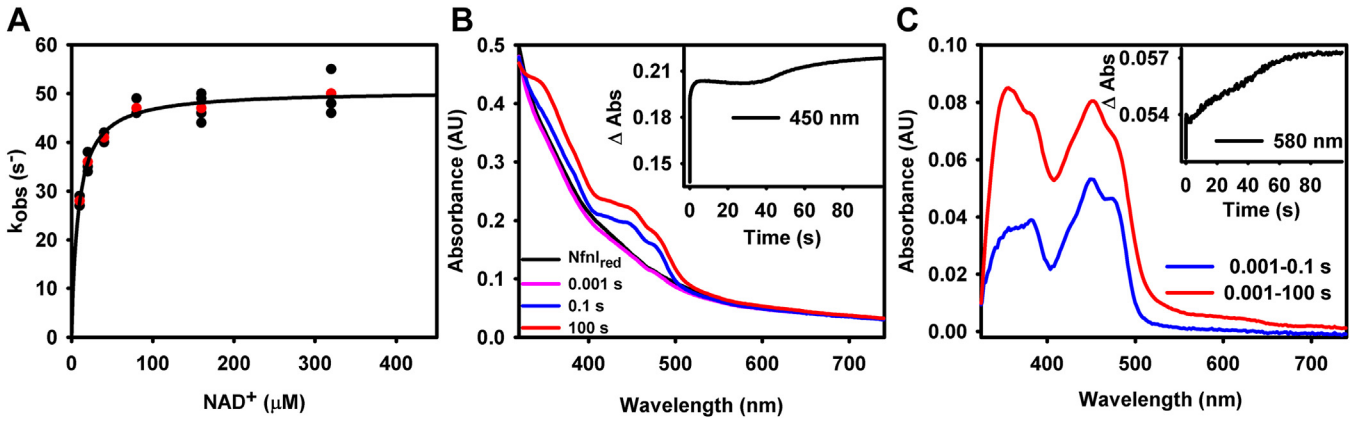

Figure 9. The oxidative half-reaction of $NfnI_{red}$ with NAD^+ at pH 9.5. Five micromolars of NfnI was pre-reduced with sodium dithionite prior to the rapid reaction experiments. *A*, plot of k_{obs} *versus* [NAD^+] with the red points indicating the average of the separate trials. The hyperbolic fit yielded a k_{ox} of 50 ± 0.7 s^{-1} and apparent K_d of 8 ± 0.6 μM. The 450 nm transients were well described by a single phase indicating that only the S-FAD was oxidized in the fast phase of the reaction. *B*, the oxidation of 5 μM NfnI pre-reduced with sodium dithionite with 5 μM NAD^+. The spectrum of the reduced NfnI (*black*), first point collected (*magenta*), the end of the 100 ms fast phase (*blue*), and the end time point (*red*). *Inset:* the 450 nm transient of the oxidation of the S-FAD over the 100 s time period, most notably showing that much of the absorption change is due to the fast phase of the oxidation. *C*, the difference spectra generated by subtracting the spectra at time points from panel *B* shown in the figure legend. FADH• begins to accumulate on a time scale of seconds with maximum accumulation by 100 s (*red* spectrum). *Inset:* the 580 nm transient tracking the formation of the FADH•.

Discussion

As expected, the reductive half-reaction of NfnI with excess NADPH is multiphasic, with three successive equivalents of NADPH reacting in turn to fully reduce the protein. At pH 7.5, the apparent limiting k_{red} of the initial reduction is ∼113 ± 7.6 s^{-1} with tight binding as reflected in an apparent K_d of 8 ± 2.8 μM. The reaction is somewhat slower at pH 9.5 with an apparent k_{red} of 36 ± 1.6 s^{-1} but the apparent K_d is similar at 5 ± 1.2 μM. The low apparent K_d values seen here from the kinetics of the reaction are consistent with previous results of fluorescence titrations at pH 8.8 indicating a K_d of 3 μM (5). The multiple phases of the reaction at both pH values are similar in nature: an initial phase having a spectral change dominated by flavin reduction occurs within 150 ms reflecting reduction of the L-FAD by NADPH, with a subsequent intermediate phase that includes reduction of the S-FAD (detected *via* the absorbance around 600 nm of the FADH• that forms upon a single electron reduction of the S-FAD which accumulates maximally at ∼5 s). The slowest phase of reduction can be attributed to the reduction of the low-potential [4Fe-4S] clusters, not easily monitored *via* UV/visible spectrophotometry but unequivocally established by EPR. The slow reduction of the low potential [4Fe-4S] clusters is evidence of gated bifurcation activity by the sluggish electron transfer that occurs in the high-potential pathway in the absence of NAD^+, as the reducing power needed for electron transfer to the proximal [4Fe-4S] cluster is produced upon formation of the L-FAD•$^-$. The more complete reduction of NfnI seen at higher pH reflects the stronger reducing power of NADPH at higher pH.

NfnI catalyzes electron bifurcation such that the steady-state reduction of ferredoxin and NAD^+ are tightly coupled. Nevertheless, the rapid-reaction kinetic experiments described here demonstrate that ferredoxin is reduced in the course of reduction of NfnI by NADPH in the absence of NAD^+. A significant amount of ferredoxin becomes reduced within a second upon mixing a solution of NfnI and ferredoxin with excess NADPH, although most ferredoxin reduction occurs on a much slower time scale than steady-state catalysis. Under steady state conditions, in the presence of NAD^+, the reaction is over within 100 s, while in the absence of NAD^+, the reaction approaches completion at 600 s. The extent of ferredoxin reduction is pH-dependent, with the ratio of ferredoxin reduced to NfnI approaching a maximum of 3:1 at pH 9.5. At pH 7.5, the lower yield of reduced ferredoxin appears to be due to a combination of the weaker effectiveness of NADPH as reductant and a certain amount of reverse electron transfer from the reduced ferredoxin back to NfnI. The back electron transfer is a product of NfnI being able to make NADPH from reduced ferredoxin and NADH in a confurcating reaction and is evidenced by the reoxidation at 420 nm in the inset of Figure 4*B* (pink) (3). In the course of the reductive half-reaction of NfnI in the presence of ferredoxin at the higher pH, three successive equivalents of NADPH can react, each sending one electron into the high- and low-potentials pathways, before the high-potential pathway fills up in the absence of NAD^+ (the [2Fe-2S] cluster and S-FAD being able to take up a total of three electrons). Concomitantly, low-potential electrons enter the low-potential pathway, ultimately removed by ferredoxin. Thus, a theoretical maximum of three low-potential electrons for ferredoxin reduction can be generated under these conditions, a maximum that is approached at pH 9.5. These results indicate that the tight coupling of bifurcation is an intrinsic property of the bifurcating L-FAD of NfnI and not strictly dependent on the presence of the high-potential acceptor NAD^+.

The high efficiency of electron bifurcation means that the low-potential electrons generated in successive bifurcation events do not leak into the high-potential pathway to any significant degree, although this process must be strongly favorable thermodynamically. Since electron leakage does not occur on the tens of seconds time scale of ferredoxin reduction at pH 9.5 in the experiments reported here, the implication is that such leakage must be very slow and appears to be due to inefficient electron transfer into the high-potential pathway in the absence of NAD^+. In the presence of NAD^+, ferredoxin reduction, and by implication of electron transfer into the low-potential pathway, becomes much faster as the rate-limiting transfer of the first, high-potential electron into the high-potential pathway increases. Both crystallographic (3) and H/D exchange mass spectrometric (4, 8, 9) work has suggested a subtle conformational change along the polypeptide backbone between the L-FAD and [2Fe-2S] cluster of the high-potential pathway upon binding NAD^+ that alters the binding of the aspartate ligand to the cluster from bidentate to monodentate, which may well facilitate electron transfer into the high-potential pathway in the presence of NAD^+. This subtle conformational change, while potentially important, does not resemble the very large domain motions seen in other bifurcating systems possessing an electron-transferring flavoprotein (11).

NfnI is also reduced by NADH in the reverse of the bifurcation reaction, for example, in the confurcation direction. The reductive half-reaction with NADH exhibits a well-behaved fast phase with a spectral change consistent with reduction of the S-FAD. The observed rate constant exhibits hyperbolic dependence of [NADH] with a k_{red}^{app} of 205 ± 1.9 s^{-1} and an apparent K_d of 29 ± 1.1 μM. After a reproducible "lag" portion after the end of the fast phase that lasts for 1 s, the enzyme becomes further reduced, reflecting at least partial electron transfer to the [2Fe-2S] cluster of the high-potential pathway. S-FADH• accumulates in this phase of the reaction along with reduced [2Fe-2S] cluster, as confirmed by EPR. This slower phase thus appears to represent the establishment of an equilibrium in the high-potential pathway containing two reducing equivalents, with one distribution favoring full reduction of the S-FADH$^-$ and oxidized [2Fe-2S] cluster and the second S-FADH• and reduced [2Fe-2S] cluster.

NADH-reduced NfnI is able to reduce ferredoxin, albeit at rates slower than seen with NADPH-reduced protein (Fig. S4). Although electron transfer from the high-potential pathway to the bifurcating L-FAD to give L-FADH$^-$ is possible, it seems more likely that NADH is able to bind to and reduce the L-FAD directly, in which case electron bifurcation would occur normally as with NADPH. Indeed, H/D exchange mass

spectrometry has provided evidence that NADH can bind at the L-FAD (8, 9).

Lastly, in considering the oxidative half-reaction, we find that NAD^+ can effectively oxidize the S-FAD of dithionite-reduced NfnI, as expected, with the observed rate constant exhibiting hyperbolic dependence on [NAD^+] from which a k_{red}^{app} of 50 ± 0.7 s^{-1} and apparent K_d of 8 ± 0.6 μM has been determined. The spectral change associated with the observed kinetics indicates that only the S-$FADH^-$ becomes oxidized, with the other redox-active centers remaining reduced, again reflecting little leakage of low-potential reducing equivalents into the high-potential pathway on the time scale of the observed kinetics. Electron transfer from the reduced [2Fe-2S] cluster to the oxidized S-FAD is evident in the formation of S-FADH• during the oxidative half-reaction with NAD^+, as reflected in the increase in absorbance at around 600 nm. Figure 9*C* shows that after the initial oxidation of the S-FAD, S-FADH• begins to form only on a tens of seconds time scale and not immediately upon oxidation of the S-FAD. To the extent that the [2Fe-2S] cluster remains reduced, it would effectively block transfer of low-potential electrons into the high-potential pathway, thereby ensuring tightly coupled bifurcation.

In conclusion, the work here demonstrates that bifurcation is an intrinsic property of the L-FAD of NfnI and that reduction of ferredoxin occurs even in the absence of NAD^+, albeit slowly. NAD^+ greatly accelerates the rate of ferredoxin reduction, likely by triggering a previously identified conformational change that facilitates the rate-limiting electron transfer into the high-potential pathway. Electron transfer into and along the low potential pathway to a docked ferredoxin does not appear to limit the rate of bifurcation during catalysis and is evidenced by the ability of pre-reduced NfnI (with at least one electron in the low-potential pathway) to rapidly transfer an electron to oxidized ferredoxin, yielding approximately a full equivalent worth of reduced ferredoxin. Electron transfer into the low-potential pathway is known to occur on a picosecond time scale (4) and is not rate-limiting in catalysis. The factors governing the rate of electron transfer into the high-potential pathway appears to be key to understanding the gating of electron bifurcation in NfnI. Future work will focus on examining the possible role of proton-coupled events in the initial election transfer out of the bifurcating L-$FADH^-$ to the [2Fe-2S] cluster of the high-potential pathway, as well as the subsequent electron on to the S-FAD (initially yielding the neutral FADH•).

Experimental procedures

Organisms and growth conditions for ferredoxin from M. elsdenii *and* P. furiosus

Ferredoxin from either *M. elsdenii* (NCBI: locus tag C6Y28_RS04440) or *P. furiosus* (12) was overexpressed in *Escherichia coli* cell line CLK002 (MG1655 *Δisc ΔmetJ*; Frank Sargent, Newcastle University, personal communication). Both plasmids were constructed so as to have an N-terminal Strep-II tag and were treated identically. Cells were grown on TGYEP-rich media, supplemented with 0.8% glycerol. An 80 ml preculture was grown overnight with 100 μg/ml ampicillin at 30 °C while being shaken at 220 rpm. Three liters of TGYEP media, also containing 100 μg/ml ampicillin, in a 6 L flask was inoculated with the preculture to a starting A_{600} of 0.2 and shaken at 30 °C at 180 rpm. Once the A_{600} of the aerobic portion of the growth reached an A_{600} between 1.5 to 1.8, the cells were transferred to another 3 L flask for the anaerobic portion of the growth. After transfer, 2 mM IPTG and 100 μl of Antifoam B emulsion (Sigma-Aldrich) were added, along with 0.25 g/L of L-cysteine and 0.2 g/L of ferric ammonium citrate. The flasks were then sealed and cells were grown anaerobically for 36 h with constant bubbling with argon; cells were harvested by centrifugation at 5500*g* at 4 °C for 20 min, frozen, and stored in liquid nitrogen until needed. A typical yield was 5 g cells/L of media.

Purification of ferredoxin from M. elsdenii *and* P. furiosus

Purification of *M. elsdenii* and *P. furiosus* ferredoxin was performed anaerobically at 4 to 10 °C in an anaerobic chamber with an atmosphere that included 2.5 to 3% H_2. The procedure for purification of both proteins was identical. Frozen cells were thawed and suspended in a lysis buffer consisting of 50 mM Tris–HCl, 150 mM NaCl, pH 8.0 supplemented with 1 mM NaF, 1 mM benzamidine, 1 mM PMSF, 10 mM glucose, lysozyme, DNase I, and catalytic amounts of glucose oxidase from *Aspergillus niger* and bovine liver catalase to scavenge residual O_2 (13). The cells were incubated in the lysis buffer for a minimum of 1 h and passed through an EmulsiFlex-B15 cell homogenizer (Avestin, Inc). The lysate was centrifuged at 42,000*g* for 30 min, and the supernatant then loaded at a rate of 0.5 ml/min onto a 5-mL Strep-Tactin XT Superflow column pre-equilibrated with 10 column volumes (CVs) of 50 mM Tris–HCl, 150 mM NaCl, pH 8.0. The column was washed with 50 mM Hepes, pH 7.5 for 20 CVs and the bound ferredoxin then eluted with the same buffer supplemented with 50 mM biotin directly onto a 1 ml Q-Sepharose column. The Q-Sepharose column was then washed with 20 CVs of 50 mM Hepes pH 7.5 and the protein eluted using the same buffer with the addition of 0.5 M NaCl. A typical yield consisted of 2 mg of *P. furiosus* or 1 mg of *M. elsdenii* ferredoxin from 30 g of cell paste. Protein aliquots were frozen and stored in liquid N_2 until further use.

Growth, overexpression, purification, and reconstitution of recombinant NfnI from P. furiosus *in* E. coli

NfnI was grown, overexpressed, purified, and reconstituted as previously reported (5). Heterologous expression of NfnI (*aka* "NfnSL") was conducted in terrific broth media with *E. coli* BL21 (DE3) harboring a $strep^R$ pCDFDuet-1 plasmid containing *nfnS* and *nfnL* genes, codon optimized by GenScript. Using an overnight starter culture with 100 μg·mL^{-1} streptomycin, 1:100 inoculum was used to inoculate individual 1 L volumes of sterile terrific broth media supplemented with 0.4% glycerol, 100 μg·mL^{-1} streptomycin sulfate, 125 μg·mL^{-1} thiamine·HCl, trace metals (50 μM $FeCl_3$, 20 μM $CaCl_3$, 10 μM $MnCl_2$, 10 μM $ZnSO_4$, 5 μM $MgSO_4$, 2 μM $CoCl_2$, 2 μM $CuCl_2$, 2 μM $NiCl_2$),

1 mM ferric ammonium citrate, and 5 μM FAD. One liter of cultures were allowed to grow at 37 °C in a shaking incubator at 250 rpm until an optical density at 600 nm of ∼0.6 was reached, in which 0.5 mM IPTG was added for induction, as well as further supplemented with FAD and ferric ammonium citrate to final concentrations of 10 μM and 2.5 mM, respectively. Cultures were allowed to incubate at 37 °C and 250 rpm for another 60 min, after which 2x 1 L cultures were combined into a septum-sealed, sterile 2 L narrow-neck flask containing 10 mM sodium fumarate and 0.5% (w/v) $_D$-glucose and allowed to incubate without shaking at room temperature for ∼30 min. Once room temperature incubation reached ∼30 min, 1 mM L-cysteine and 0.005% (v/v) Sigma-Aldrich Antifoam-289 were added, and afterward, the cultures were septum sealed and sparged with argon gas for ∼16 h at room temperature. Cultures were harvested anaerobically (97%/3% N_2/H_2) and centrifuged at 4 °C for 10 min at 6000 rpm, and cell pellets were resuspended in anoxic 150 mM Hepes, pH 8.80, 200 mM NaCl, and 5% glycerol and recentrifuged to wash them of residual growth media. Once washed, cell pellets were resuspended in aforementioned buffer, aliquoted into equal amounts, septum sealed, and stored at −80 °C until further use.

Cell lysis and NfnI purification were carried out in anoxic conditions to prevent oxidative destruction of NfnI cofactors. Each aliquot of frozen cell suspension was thawed and anoxically mixed with 75 units of Pierce Universal Nuclease, 20 mg of lysozyme, one tablet of Roche cOmplete EDTA-free Protease Inhibitor Cocktail, and ∼0.015% (v/v) of Sigma-Aldrich Antifoam-289. Cell suspensions were then lysed using an anoxic Microfluidics M-110S microfluidizer, in which the cell suspensions were passed through no less than 10 times for complete lysis (97%/3% N_2/H_2). After lysis, cell lysate was transferred to a septum-sealed vial and then heated at 75 °C for 1 hour and then ultracentrifuged (in polycarbonate bottles with aluminum cap assembly, Beckman Coulter 355618) at 4 °C at 45,000 rpm for 1 hour. Once lysate was ultracentrifuged, all ultracentrifuge bottles were transferred to an anoxic box containing 100% N_2 gas where all proceeding purification steps in this section were performed. Ultracentrifuged lysate supernatant was decanted from pelleted solids and flowed onto a high capacity Strep-Tactin XT resin (IBA Life Sciences) gravity column equilibrated with anoxic 150 mM Hepes, pH 8.80, 200 mM NaCl, 5% glycerol. Once all supernatant was flowed over the column, bound protein was washed with two CV buffer, then eluted with 5 CV of the same buffer containing 25 mM $_D$-biotin. Eluent was collected visually into fractions by hue, and fractions were assessed for purity by SDS-PAGE. Fractions deemed ≥95% pure were pooled and the protein concentration assessed *via* Bradford method. As-purified *Pf*NfnI lacks full incorporation of catalytic [Fe-S] and FAD cofactors (10 Fe and two FAD per NfnI complex) and requires reconstitution to produce a replete protein.

Cofactor reconstitution was anoxically (100% N_2) performed similar to (5) in order to produce cofactor-replete NfnI. NfnI was diluted to approximately 100 μM in 150 mM Hepes, pH 8.80, 200 mM NaCl, 5% glycerol with 1.5% beta-mercaptoethanol and incubated at room temperature and stirred for 15 min. After incubation with beta-mercaptoethanol, 2:1 FAD (200 μM) and 5:1 NAD^+ (500 μM) were added to facilitate FAD loading into NfnI and incubated at room temperature stirring for 30 min. After 30 min, 8:1 (800 μM) ferrous ammonium sulfate was added to load empty iron sites in iron-sulfur clusters in NfnI and left to incubate at room temperature, stirring for 15 min. After 15 min, 8:1 sodium sulfide (800 μM) was added to the stirring solution, left to incubate for 15 min, and then septum sealed and incubated for 18 h at 37 °C. After reconstitution, protein was desalted with a PD-10 desalting column (GE Life Sciences) and washed and concentrated using a 50 ml volume Amicon Stirred Cell (Millipore Sigma) with a 10 kDa-cutoff regenerated cellulose filter until stirred cell filtrate color was clear. Reconstituted and concentrated NfnI was stored anoxically at 4 °C.

To confirm reconstitution facilitated full cofactor loading of NfnI, iron-counting was performed as previously described (14, 15) and FAD-counting was adapted from a previous method (16). Iron-counting was performed using a ferrozine-based colorimetric assay to quantify the amount of iron associated with one equivalent of NfnI. A volume of NfnI corresponding to an estimated 1.2 μg of iron was diluted to a final volume of 1 ml in triplicate with Milli-Q ultrapure water (MilliporeSigma). An iron standard curve consisting of 0.4, 0.8, 1.2, 1.6, and 2.0 μg iron each in 1 ml Milli-Q ultrapure water was prepared concurrent to the NfnI samples using a 10 ppm (*e.g.*, 10 μg/ml) atomic absorption spectroscopy iron standard (RICCA Chemical Co). To each of the NfnI and standard curve samples, 0.5 ml of reagent A (2.25% w/v $KMnO_4$ and 0.6 M HCl) was added and then heated at 65 °C for 2 h. After the 2-h digestion, 0.1 ml of reagent B (4.85 g ammonium acetate, 4.40 g ascorbic acid, 0.04 g neocuproine, 0.04 g ferrozine, in 15 ml water total) was added to each sample and left to incubate at room temperature for 30 min. After room temperature incubation, the absorbance at 562 nm was recorded, subtracting the contribution at 900 nm. The amount of iron in the NfnI samples are compared to the standard curve and back calculated to inform the complete level of iron loading per equivalent of NfnI. FAD was quantified following digestion of NfnI. ∼5 to 10 μM NfnI was digested in 7.5 mM ascorbic acid, 0.1% trichloroacetic acid for 10 min at 95 °C and then centrifuged at 13,000 rpm in a tabletop centrifuge. The supernatant spectrum was measured, and the flavin concentration was confirmed by taking the absorbance at 446 nm and the extinction coefficient of FMN, 11.1 mM^{-1} cm^{-1}. NfnI iron loading and FAD loading were measured at 10.2 ± 0.1 iron atoms per NfnI (102%) and 1.81 ± 0.04 FAD per NfnI (90%).

Rapid-reaction kinetics of NfnI

All rapid-reaction kinetic experiments were performed at 30 °C. All solutions were prepared in an anaerobic chamber using buffer that was supplemented with 10 mM glucose and made anaerobic by bubbling with nitrogen for a minimum of 20 min. After bubbling, catalytic amounts of glucose oxidase and catalase were added to the buffer to scrub residual O_2, which was then transferred to the anaerobic chamber. Substrate

solutions were prepared in the anaerobic chamber at appropriate concentrations and transferred to glass syringes (Cadence Science) to be loaded onto the stopped-flow apparatus. NfnI samples were also prepared in the anaerobic chamber, stock solutions being diluted into appropriate volumes of 100 mM glycine, 300 mM NaCl, pH 9.5 or 50 mM Hepes, 300 mM NaCl pH 7.5, and loaded into tonometers or glass syringes to be loaded onto the stopped-flow apparatus. NfnI was stable for hours in each buffer used, as reflected in the lack of turbidity on an hourly time scale. Using an estimated extinction coefficient of ε_{450} = 50 mM^{-1} cm^{-1}, a final concentration of 5 μM NfnI was utilized in each experiment unless otherwise noted. The oxidized and fully reduced spectra in the rapid-reaction kinetic experiments were generated by mixing oxidized or reduced anaerobic enzyme in one syringe with anoxic buffer in another syringe in the stopped-flow apparatus. Rapid-reaction kinetic experiments were performed using an Applied Photophysics SX-20 stopped-flow spectrophotometer with the acquisition software package ProData SX 2.2.5.6. For the fast phase of the reduction of NfnI by NADPH, kinetic transients were collected at 450 nm at 30 °C using a photomultiplier tube detector; on longer time scales, a photodiode array detector was used to obtain full spectra at each time point. The kinetics were fit using multiple exponentials using software provided by the manufacturer.

Electron paramagnetic resonance

EPR experiments were performed at 15K with a Bruker Magnettech ESR 5000 fitted with a LTR-MS-5000 liquid Helium cryostat (Advanced Research Systems) and a Lakeshore 335 variable temperature controller. A 50 μM *M elsdenii* Fd_{red} standard was prepared using excess dithionite; the sample was left overnight to ensure full reduction, as judged by UV/visible spectroscopy. EPR samples that contained NfnI and ferredoxin were kept at a 1:5 ratio and with saturating concentrations of NADPH and/or NAD^+ as appropriate. Samples were heated in a water bath at 30 °C for 10 min before reactions, and proteins were mixed in order to mimic the conditions of the rapid-reaction kinetic experiments. In addition, the time points selected for freezing samples were correlated with the kinetic phases seen in the stopped-flow experiments, for example, the end of the fast phase of the reaction and the most reduced time point of the 450 nm transient. The resulting EPR spectra were compared to the EPR spectrum of a fully reduced 50 μM *M elsdenii* ferredoxin standard in order to quantify the amount of ferredoxin reduced under each condition.

The $NfnI_{red}$ and oxidized ferredoxin samples were made by anaerobically pre-reducing the NfnI with sodium dithionite in the anaerobic chamber, monitoring reduction spectrophotometrically over 2 hours until there was no excess dithionite present at 314 nm. Sodium dithionite was titrated in the enzyme solution from a 2 mM stock until full reduction of NfnI was obtained. To ensure efficient mixing, oxidized ferredoxin was added to the bottom of an anaerobic EPR tube, and the tube was then septum-sealed and $NfnI_{red}$ added using an air-tight Hamilton syringe. Thus, samples were rapidly mixed and frozen in an ethanol/dry ice bath in <1 s.

Steady-state ferredoxin assays

Solutions for steady-state assays were prepared in the anaerobic chamber using nitrogen-bubbled buffers in septum-sealed cuvettes. The assay mix consisted of 0.01 μM NfnI, 25 μM ferredoxin, 1 mM NAD^+, and 0.5 mM NADPH, the NfnI and ferredoxin having been preincubated together in the cuvette while the other substrates were added *via* a sealed Hamilton syringe to begin the assay. Each assay was performed at 80 °C and the cuvettes were allowed to equilibrate with respect to temperature for 8 min before addition of substrates. The reaction was monitored at 426 nm following ferredoxin reduction over a period of 5 min; an extinction change of $\varepsilon_{426\ nm}$ = 13.1 mM^{-1} cm^{-1} was used (4). The steady-state assays were used to ascertain for the percentage of active protein in each preparation of NfnI that was used.

Data availability

Data not contained in the article (protein gels, absorption spectra, and raw rapid-reaction data) are available on request to the corresponding author (russ.hille@ucr.edu).

Supporting information—This article contains supporting information.

Acknowledgments—Work in RH's laboratory was supported by the Department of Energy (DE-SC00010666). C. E. L. is the recipient of an award from the Early Career Research Program of the Office of Science, Department of Energy. The views expressed in the article do not necessarily represent the views of the DOE or the U.S. Government. The U.S. Government retains and the publisher, by accepting the article for publication, acknowledges that the U.S. Government retains a nonexclusive, paid-up, irrevocable, worldwide license to publish or reproduce the published form of this work, or allow others to do so, for U.S. Government purposes. The authors would also like to thank Professor Frank Sargent from Newcastle University for the generous donation of the CLK002 cell line used to express the recombinant *M.e.* and *P.f.* ferredoxins used in this work. The authors would like to thank Wayne Vigil for both the *M.e.* and the *P.f.* ferredoxin UV/visible spectra presented in the Fig. S2 and Courtney Wise for a preparation of *P.f.* NfnI.

Author contributions—S. O. and D. N. methodology; S. O. and S. W. investigation; S. O. and R. H. writing–original draft; C. E. L. and R. H. resources; R. H. conceptualization; D. N., C. E. L., and S. W. writing–review and editing; D. N. and C. E. L. supervision.

Funding and additional information—This work was authored in part by the National Renewable Energy Laboratory, operated by Alliance for Sustainable Energy, LLC, for the U.S. Department of Energy (DOE) under Contract No. DE-AC36-08GO28308 with funding provided by the U.S. DOE Office of Science to C. E. L. and S. W. This work as also supported by DOE grant DE-SC0010666 (to R. H.).

Conflict of interest—The authors declare that they have no conflicts of interest with the contents of this article.

Abbreviations—The abbreviations used are: CV, column volume; EPR, electron paramagnetic resonance.

References

1. Buckel, W., and Thauer, R. K. (2018) Flavin-based electron bifurcation, A new mechanism of biological energy coupling. *Chem. Rev.* **118**, 3862–3886
2. Peters, J. W., Beratan, D. N., Bothner, B., Dyer, R. B., Harwood, C. S., Heiden, Z. M., *et al.* (2018) A new era for electron bifurcation. *Curr. Opin. Chem. Biol.* **47**, 32–38
3. Demmer, J. K., Huang, H., Wang, S. N., Demmer, U., Thauer, R. K., and Ermler, U. (2015) Insights into flavin-based electron bifurcation *via* the NADH-dependent reduced ferredoxin:NADP oxidoreductase structure. *J. Biol. Chem.* **290**, 21985–21995
4. Lubner, C. E., Jennings, D. P., Mulder, D. W., Schut, G. J., Zadvornyy, O. A., Hoben, J. P., *et al.* (2017) Mechanistic insights into energy conservation by flavin-based electron bifurcation. *Nat. Chem. Biol.* **13**, 655–659
5. Wise, C. E., Ledinina, A. E., Mulder, D. W., Chou, K. J., Peters, J. W., King, P. W., *et al.* (2022) An uncharacteristically low-potential flavin governs the energy landscape of electron bifurcation. *Proc. Natl. Acad. Sci. U. S. A.* **119**, e2117882119
6. Nitschke, W., and Russell, M. J. (2012) Redox bifurcations: mechanisms and importance to life now, and at its origin. *Bioessays* **34**, 106–109
7. Chenault, H. K., and Whitesides, G. M. (1987) Regeneration of nicotinamide cofactors for use in organic synthesis. *Appl. Biochem. Biotechnol.* **14**, 147–197
8. Demmer, J. K., Rupprecht, F. A., Eisinger, M. L., Ermler, U., and Langer, J. D. (2016) Ligand binding and conformational dynamics in a flavin-based electron-bifurcating enzyme complex revealed by Hydrogen-Deuterium Exchange Mass Spectrometry. *FEBS Lett.* **590**, 4472–4479
9. Berry, L., Poudel, S., Tokmina-Lukaszewska, M., Colman, D. R., Nguyen, D. M. N., Schut, G. J., *et al.* (2018) H/D exchange mass spectrometry and statistical coupling analysis reveal a role for allostery in a ferredoxin-dependent bifurcating transhydrogenase catalytic cycle. *Biochim. Biophys. Acta Gen. Subj.* **1862**, 9–17
10. Conover, R. C., Kowal, A. T., Fu, W., Park, J. B., Aono, S., Adams, M. W. W., *et al.* (1990) Spectroscopic characterization of the novel iron-sulfur cluster in *Pyrococcus furiosus* ferredoxin. *J. Biol. Chem.* **265**, 8533–8541
11. Demmer, J. K., Chowdhury, N. P., Selmer, T., Ermler, U., and Buckel, W. (2017) The semiquinone swing in the bifurcating electron transferring flavoprotein/butyryl-CoA dehydrogenase complex from Clostridium difficile. *Nat. Commun.* **8**, 1577
12. Aono, S., Bryant, F. O., and Adams, M. W. W. (1989) A novel and remarkably thermostable ferredoxin from the hyperthermophilic archaebacterium *Pyrococcus furiosus*. *J. Bacteriol.* **171**, 3433–3439
13. Vigil, W., Tran, J., Niks, D., Schut, G. J., Ge, X. X., Adams, M. W. W., *et al.* (2022) The reductive half-reaction of two bifurcating electron-transferring flavoproteins: evidence for changes in flavin reduction potentials mediated by specific conformational changes. *J. Biol. Chem.* **298**, 101927
14. Fish, W. W. (1988) Rapid colorimetric method for the quantitation of complexed iron in biological samples. *Methods Enzymol.* **158**, 357–364
15. Riemer, J., Hoepken, H. H., Czerwinska, H., Robinson, S. R., and Dringen, R. (2004) Colorimetric ferrozine-based assay for the quantitation of iron in cultured cells. *Anal. Biochem.* **331**, 370–375
16. Aliverti, A., Curti, B., and Vanoni, M. A. (1999) Identifying and quantitating FAD and FMN in simple and in iron-sulfur-containing flavoproteins. *Flavoprotein Protoc.* **131**, 9–23
17. Strickland, S., Palmer, G., and Massey, V. (1975) Determination of dissociation constants and specific rate constants of enzyme-substrate (or protein-ligand) interactions from rapid reaction kinetic data. *J. Biol. Chem.* **250**, 4048–4052